nature cell biology

SUPPLEMENTARY INFORMATION

https://doi.org/10.1038/s41556-019-0374-6

In the format provided by the authors and unedited.

Kinetically distinct phases of tau on microtubules regulate kinesin motors and severing enzymes

Valerie Siahaan[1,5], Jochen Krattenmacher[1,5], Anthony A. Hyman[2,3,6], Stefan Diez[2,3,4,6], Amayra Hernández-Vega[2,6]*, Zdenek Lansky[1,6]* and Marcus Braun[1,4,6]*

[1]Institute of Biotechnology of the Czech Academy of Sciences, BIOCEV, Prague West, Czech Republic. [2]Max Planck Institute of Molecular Cell Biology and Genetics, Dresden, Germany. [3]Cluster of Excellence Physics of Life, Technische Universität Dresden, Dresden, Germany. [4]B CUBE—Center for Molecular Bioengineering, Technische Universität Dresden, Dresden, Germany. [5]These authors contributed equally: Valerie Siahaan, Jochen Krattenmacher. [6]These authors jointly supervised this work: Anthony A. Hyman, Stefan Diez, Amayra Hernández-Vega, Zdenek Lansky, Marcus Braun. *e-mail: hernande@mpicbg.de; zdenek.lansky@ibt.cas.cz; marcus.braun@ibt.cas.cz

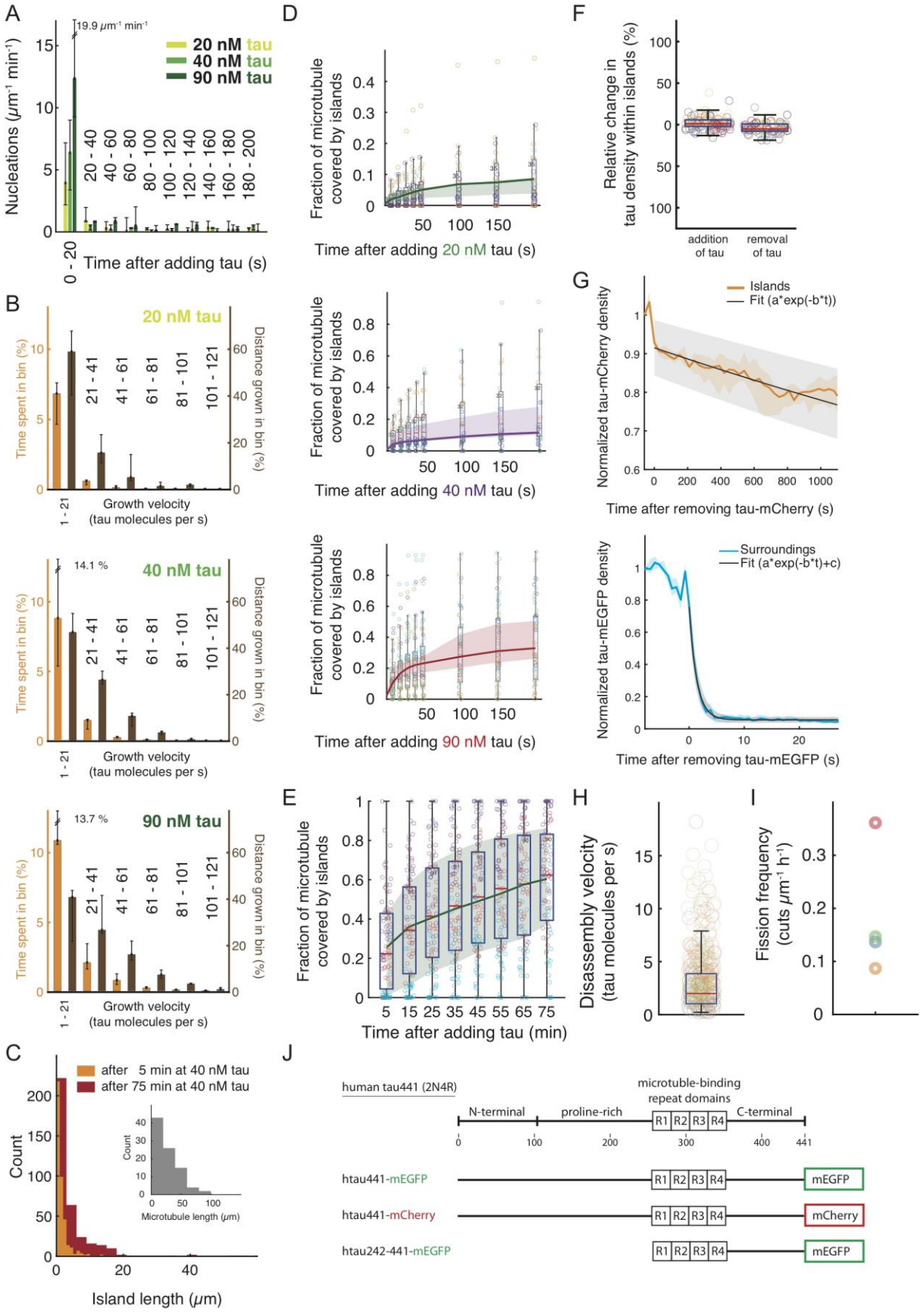
A
19.9 μm⁻¹ min⁻¹
20 nM tau
40 nM tau
90 nM tau
Nucleations (μm⁻¹ min⁻¹)
0 - 20
20 - 40
40 - 60
60 - 80
80 - 100
100 - 120
120 - 140
140 - 160
160 - 180
180 - 200
Time after adding tau (s)
B
20 nM tau
Time spent in bin (%)
Distance grown in bin (%)
1 - 21
21 - 41
41 - 61
61 - 81
81 - 101
101 - 121
Growth velocity
(tau molecules per s)
14.1 %
40 nM tau
13.7 %
90 nM tau
C
after 5 min at 40 nM tau
after 75 min at 40 nM tau
Count
Microtubule length (μm)
Island length (μm)
D
Fraction of microtubule covered by islands
Time after adding 20 nM tau (s)
Time after adding 40 nM tau (s)
Time after adding 90 nM tau (s)
E
Time after adding tau (min)
F
Relative change in tau density within islands (%)
addition of tau
removal of tau
G
Islands
Fit (a*exp(-b*t))
Normalized tau-mCherry density
Time after removing tau-mCherry (s)
Surroundings
Fit (a*exp(-b*t)+c)
Normalized tau-mEGFP density
Time after removing tau-mEGFP (s)
H
Disassembly velocity (tau molecules per s)
I
Fission frequency (cuts μm⁻¹ h⁻¹)
J
human tau441 (2N4R)
microtuble-binding repeat domains
N-terminal
proline-rich
R1
R2
R3
R4
C-terminal
htau441-mEGFP
htau441-mCherry
htau242-441-mEGFP
mEGFP
mCherry

Supplementary Figure 1

(**A)** Distribution of time between the addition of tau-mEGFP and the formation of the islands (3 experiments per condition, n = 610 nucleation events). Bars show the median; error bars show the minimum and the maximum value. Same experiments as presented in (B) and (D). **(B)** Histograms of island growth velocities at different tau concentrations in solution (Methods, n = 2131 velocity traces). Same experiments and data representation as in (A). **(C)** Distribution of the lengths of islands 5 and 75 minutes after the addition of 40 nM tau-mEGFP, n = 91 microtubules in 3 experiments. Distribution of microtubule lengths is shown in the inset. Same experiments as presented in (E). **(D)** Fraction of microtubule length covered by tau islands at different concentrations of tau-mEGFP in solution. Solid lines and shaded areas (shown also in Figure 1E) represent the median, minimum and maximum values calculated over the whole fields of view (n = 3 experiments). Boxplots represent the same statistics calculated over individual microtubules (n = 40 microtubules for 20 nM tau, n = 32 microtubules for 40 nM tau and n = 59 microtubules for 100 nM tau). The same data as presented in Figure 1E, same experiments as presented in (A). **(E)** Island assembly does not cease even 75 minutes after the addition of 20 nM tau. The same data representation as in (D), same experiments as presented in (C). (**F**) Relative difference in tau density within islands i) just after the island nucleation upon the addition of tau and 30 seconds later and ii) just after the removal of tau and 30 seconds later (n = 91 microtubules in 16 experiments). Bleaching was not negligible in the case where tau was absent from solution – for a precise estimation of tau unbinding see (G). (**G**) Exemplary time-trace of tau-mCherry density inside and tau-mEGFP density outside the islands after removal of tau (mCherry- or mEGFP-labeled, respectively) from solution, analogous to the results presented in Figure 1H (n = 6 microtubules). Single exponential fits are indicated by solid lines. This experiment had been repeated 4 and 3 times for islands and surroundings, respectively, with similar results. Time constants derived from fits for all experiments are shown in Figures 2B and Supplementary Fig. 2d. **(H)** Distribution of island disassembly velocities upon removal of tau from solution yielding the average velocity of 6.6 ± 5.2 nm/s (average ± SD, corresponding to 2.9 ± 2.3 tau molecules unbinding per second, Methods). Colors encode experiments (n = 335 velocity traces on 90 islands in 4 experiments). For a description of all boxplot elements see Methods. **(I)** Frequency of fissions occurring within islands upon removal of tau from solution yielding the average 0.20 ± 0.14 fissions per micron of island length per hour (average ± SD). Colors encode n = 4 experiments - same as in (H). **(J)** Schematics showing the tau constructs used in this study.

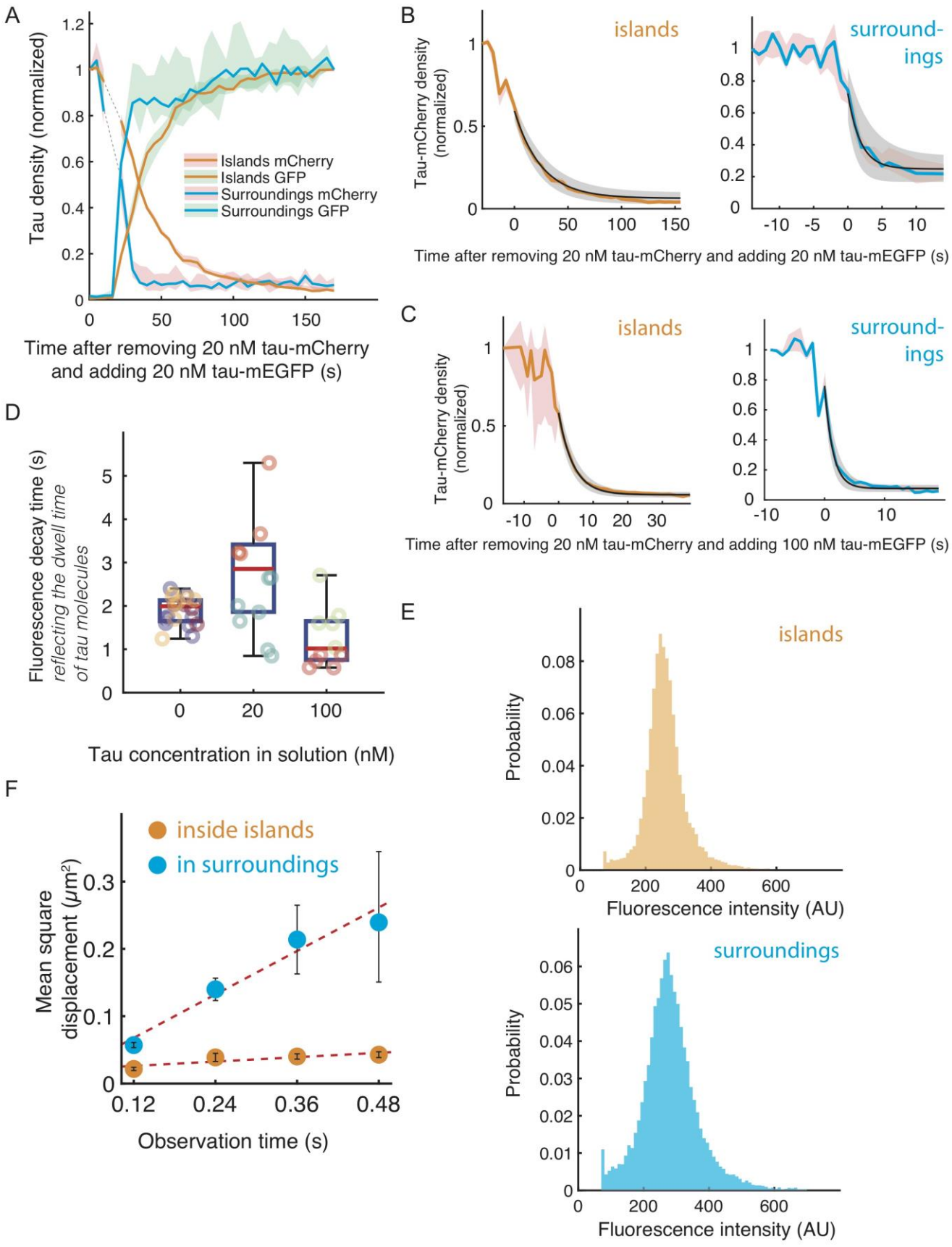
A
Tau density (normalized)
Islands mCherry
Islands GFP
Surroundings mCherry
Surroundings GFP
Time after removing 20 nM tau-mCherry and adding 20 nM tau-mEGFP (s)
B
islands
surround-ings
Tau-mCherry density (normalized)
Time after removing 20 nM tau-mCherry and adding 20 nM tau-mEGFP (s)
C
islands
surround-ings
Tau-mCherry density (normalized)
Time after removing 20 nM tau-mCherry and adding 100 nM tau-mEGFP (s)
D
Fluorescence decay time (s)
reflecting the dwell time of tau molecules
Tau concentration in solution (nM)
E
islands
Probability
Fluorescence intensity (AU)
surroundings
Probability
Fluorescence intensity (AU)
F
inside islands
in surroundings
Mean square displacement (μm²)
Observation time (s)

Supplementary Figure 2

(**A**) Exemplary time-trace of normalized tau-mCherry and tau-mEGFP density inside and outside the islands after exchange of 20 nM tau-mCherry for 20 nM tau-mEGFP (n = 5 microtubules). Photo-bleaching during this experiment was negligible (Methods). The dotted line indicates that the sample was out of focus at the time. **(B)** Exemplary time-trace and fit of tau-mCherry density inside and outside the islands after exchange of 20 nM tau-mCherry for 20 nM tau-mEGFP (n = 5 respectively 7 microtubules). Photo-bleaching during these experiments was negligible (Methods). This experiment had been repeated 5 and 2 times for islands and surroundings, respectively, with similar results. Time constants derived from fits for all experiments are shown in Figures 2B and Supplementary Fig. 2d. **(C)** Analogous estimation of tau residence times as in (B) for an exemplary experiment in which 20 nM tau-mCherry was exchanged for 100 nM tau-mEGFP (n = 5 microtubules). The photo-bleaching during this experiment was negligible (Methods). This experiment had been repeated 4 and 2 times for islands and surroundings, respectively, with similar results. Time constants derived from fits for all experiments are shown in Figures 2B and Supplementary Fig. 2d. **(D)** Boxplots of dwell times of tau outside the islands at different tau concentrations in solution (at 0 nM tau, dwell time was 1.9 ± 0.3 s, average ± SD, n = 20 microtubules in 3 experiments, at 20 nM tau, the dwell time was 2.7 ± 1.3 s, average ± SD, n = 11 microtubules in 2 experiments, for 100 nM tau, the dwell time was 1.2 ± 0.7 s, average ± SD, n = 10 microtubules in 2 experiments; for dwell times within islands see Figure 2B). Typical fits and time-traces underlying these data are shown in (B) and (C) and in Figure S1G. The data points are color-coded by experiments. For a description of all boxplot elements see Methods. **(E)** Histogram of fluorescence intensities of single tau-mEGFP particles bound to microtubules in experiments as presented in Figure 2C, showing that tau-mEGFP is associated with the microtubule in monomeric form (n = 1861 molecules inside the islands, n = 2210 molecules outside the islands, 1 experiment). **(F)** Mean square displacement over time of single tau-EGFP molecules inside and outside the islands yielding tau diffusion constants of 0.27 ± 0.15 $\mu m^2 s^{-1}$ (linear fit coefficient ± 95% confidence bounds, n = 3660 molecules, 3 experiments) outside the islands and 0.027 ± 0.016 $\mu m^2 s^{-1}$ (linear fit coefficient ± 95% confidence bounds, n = 2558 molecules, 3 experiments) inside the islands. For comparison, the analogously estimated diffusion constant of non-motile kinesin-1 molecules tightly bound to the microtubule in the presence of AMP-PNP (in the absence of ATP) was 0.014 ± 0.016 $\mu m^2 s^{-1}$ (linear fit coefficient ± 95% confidence bounds, n = 126 molecules, 1 experiment).

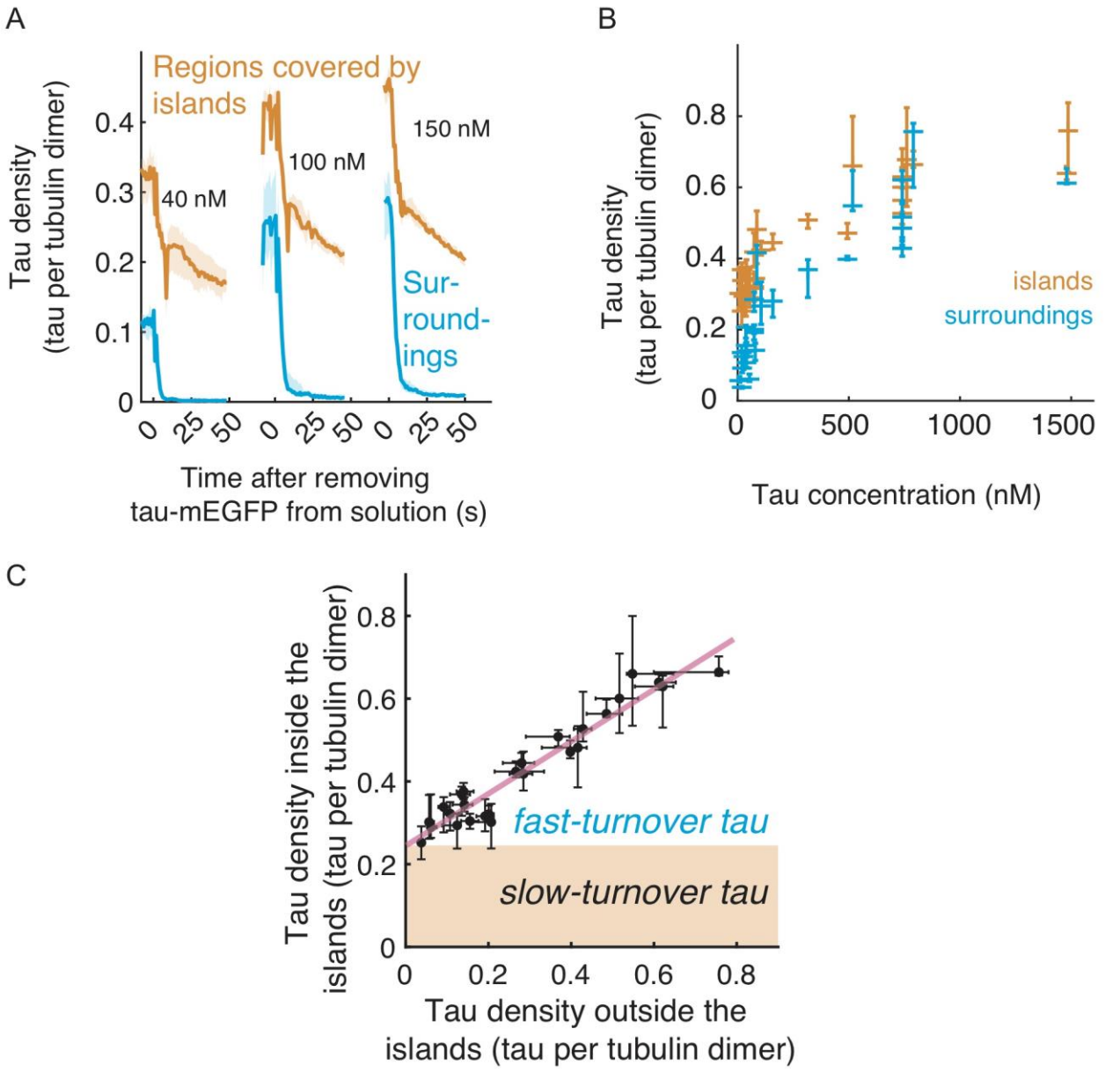

Supplementary Figure 3

(A) Exemplary time-traces of tau-mEGFP density outside and inside the islands during subsequent cycles of i) addition of increasing concentrations of tau-mEGFP followed by ii) removal of tau-mEGFP from solution. Experiment such as presented in Figure 3C. This experiment had been repeated 11 times with similar results. (B) The density of tau-mEGFP on the microtubules saturates at high (µM) tau-mEGFP concentrations (total of 29 and 27 experiments for islands and surroundings, respectively). Horizontal lines indicate the three quartiles. (C) At tau-mEGFP concentrations in the range of 20 nM to approximately 1 µM, the tau-mEGFP density inside the islands scales linearly with the tau-mEGFP density outside the islands. Points indicate medians, error bars indicate the first and third quartiles (both axes). Data from the experiments presented in (B).

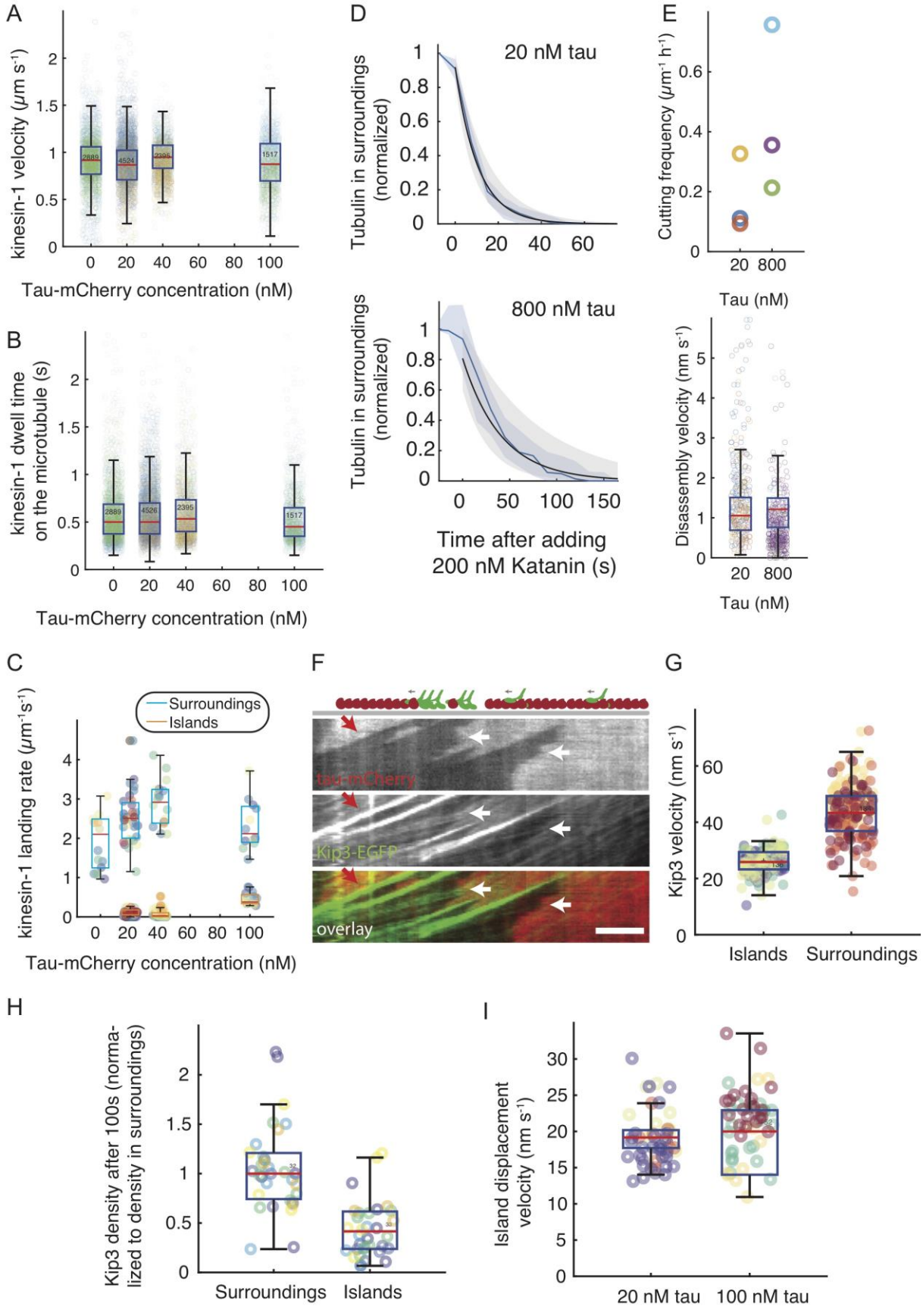
A
kinesin-1 velocity (μm s-1)
Tau-mCherry concentration (nM)
B
kinesin-1 dwell time on the microtubule (s)
Tau-mCherry concentration (nM)
C
kinesin-1 landing rate (μm-1s-1)
Surroundings
Islands
Tau-mCherry concentration (nM)
D
20 nM tau
Tubulin in surroundings (normalized)
800 nM tau
Time after adding 200 nM Katanin (s)
E
Cutting frequency (μm-1 h-1)
Tau (nM)
Disassembly velocity (nm s-1)
Tau (nM)
F
tau-mCherry
Kip3-EGFP
overlay
G
Kip3 velocity (nm s-1)
Islands
Surroundings
H
Kip3 density after 100s (normalized to density in surroundings)
Surroundings
Islands
I
Island displacement velocity (nm s-1)
20 nM tau
100 nM tau

Supplementary Figure 4

Velocities **(A)** and dwell times **(B)** of kinesin-1 molecules moving processively outside the islands formed at various tau-mCherry concentrations in solution (3 experiments at 0 nM, 6 experiments at 20 nM, 5 experiments at 40 nM, 3 experiments at 100 nM; numbers of molecules shown in box; no processive movement was observed inside the islands). **(C)** Kinesin-1 landing rates inside and outside the islands formed at various tau-mCherry concentrations in solution (7 experiments at 0 nM, 10 experiments at 20 nM, 7 experiments at 40 nM, 6 experiments at 100nM). **(D)** Exemplary time-traces of normalized tubulin signal of the regions surrounding the islands (blue line) decaying during its katanin-mediated disassembly. Single exponential fits to the data (black lines) yield a tubulin residence time of 17 ± 6.4 s (average ± S.D., n = 17 microtubules in 2 experiments) in presence of 20 nM tau-mCherry and 34 ± 23 s (average ± S.D., n = 18 microtubules in 2 experiments) in presence of 800 nM tau-mCherry. Photo-bleaching during this experiment was negligible (Methods). **(E)** Boxplot of katanin-mediated disassembly velocities of stretches of microtubules covered by tau islands (evaluated per island boundary) and the rate of katanin-generated cuts occurring within them. Experiments had been conducted at two different concentrations of tau in solution (3 experiments per condition, n = 56 microtubules at 20 nM tau and 33 at 800 nM tau). **(F)** Multichannel fluorescence kymograph showing the motion of kip3-GFP (green) inside and outside the tau islands (red). Red arrow indicates the accumulation of kip3-GFP in front of the island. White arrows indicate kip3-GFP molecules speeding up as they leave the island. Scale bar 2 µm. This experiment had been repeated 7 times with similar results. **(G)** Quantification of velocities of single Kip3-GFP motors moving inside and outside the islands at 10 nM tau-mCherry in solution (n = 136 Kip3-GFP molecules inside islands, n = 184 outside, 3 experiments). **(H)** Quantification of Kip3-GFP density inside and outside the islands 100 s after the addition of Kip3-GFP (n = 98 microtubules in 6 experiments). The presented Kip3-GFP densities are normalized to the median of the density in the surroundings (within the same experiment). **(I)** Velocities of Kip3-GFP-driven disassembly of tau islands established at two different tau-mCherry concentrations (3 experiments per condition, n = 46 islands at 20 nM, n = 52 islands at 100 nM). For a description of all boxplot elements see Methods.

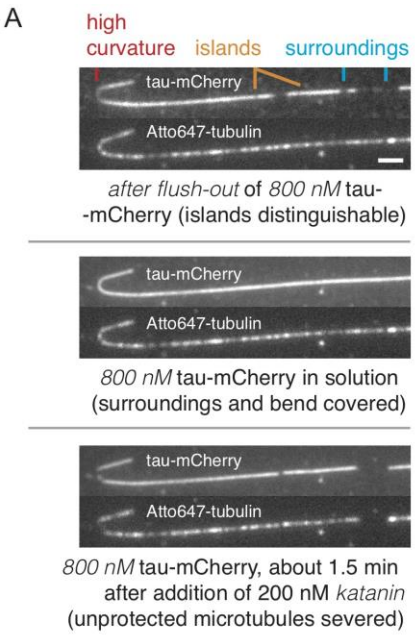
A
high curvature
islands
surroundings
tau-mCherry
Atto647-tubulin
after flush-out of 800 nM tau--mCherry (islands distinguishable)
tau-mCherry
Atto647-tubulin
800 nM tau-mCherry in solution (surroundings and bend covered)
tau-mCherry
Atto647-tubulin
800 nM tau-mCherry, about 1.5 min after addition of 200 nM katanin (unprotected microtubules severed)

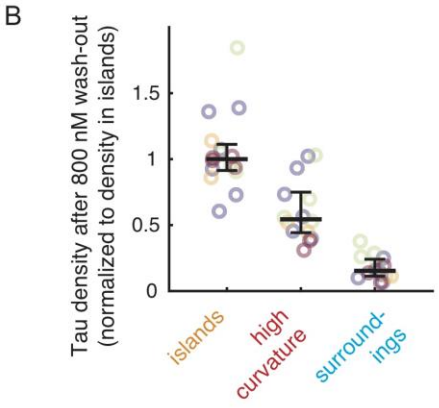
B
Tau density after 800 nM wash-out (normalized to density in islands)
1.5
1
0.5
0
islands
high curvature
surround-ings

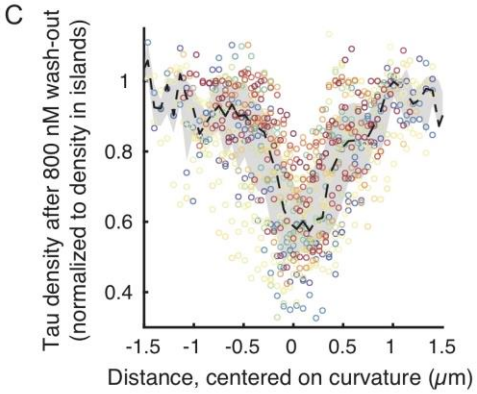
C
Tau density after 800 nM wash-out (normalized to density in islands)
1
0.8
0.6
0.4
-1.5
-1
-0.5
0
0.5
1
1.5
Distance, centered on curvature (μm)

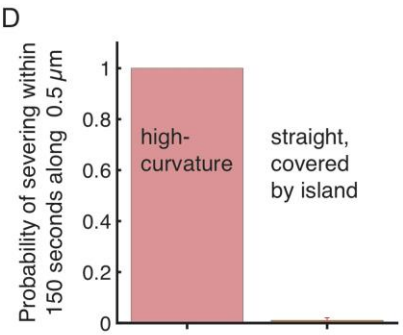
D
Probability of severing within 150 seconds along 0.5 μm
1
0.8
0.6
0.4
0.2
0
high-curvature
straight, covered by island

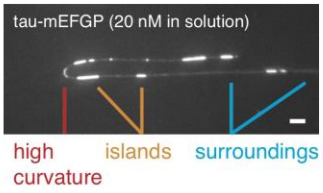
E
tau-mEFGP (20 nM in solution)
high curvature
islands
surroundings

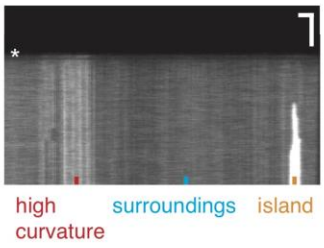
F
*
high curvature
surroundings
island

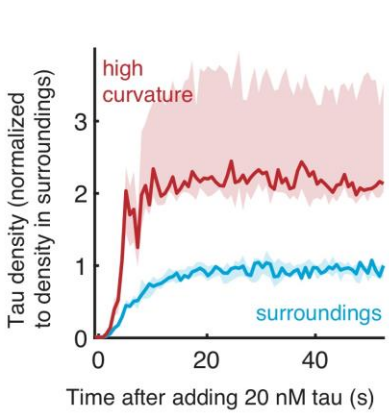
G
high curvature
surroundings
Tau density (normalized to density in surroundings)
3
2
1
0
0
20
40
Time after adding 20 nM tau (s)

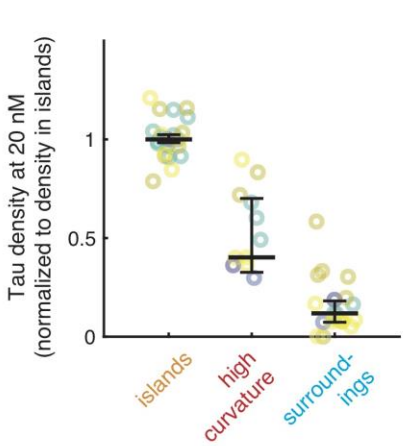
H
Tau density at 20 nM (normalized to density in islands)
1
0.5
0
islands
high curvature
surround-ings

Supplementary Figure 5

Figure S5. (A) Tau-mCherry islands on microtubules after the removal of 800 nM tau-mCherry from solution (upper panel); the same microtubule in presence of re-introduced 800 nM tau-mCherry in solution (middle panel); the same microtubule in presence of 200 nM katanin-GFP and 800 nM tau-mCherry. This experiment had been repeated 4 times with similar results. **(B)** Densities of tau-mCherry outside the islands, inside the islands and in the regions of high curvature (after the removal of 0.8 µM tau from solution). Points are color-coded by experiments (n = 15 high-curvature regions in 4 experiments), horizontal lines indicate the three quartiles, weighted such that each experiment has equal weight. **(C)** Tau density profile along the microtubule after removing 800 nM tau from solution. X-axis is centered on the point of highest curvature. Data are color-coded by microtubule and the density is normalized to the 90th percentile of the density-values of the respective microtubule. The red line represents the median of n = 30 microtubules (7 experiments), the first and third quartile are indicated by the shaded area. At 800 nM tau, there always were islands adjacent to microtubule bends, which is why the tau density to the left and right of the curved microtubule region is high even though tau has been removed from solution. A clear decrease in the tau density is apparent at the point of highest curvature. **(D)** Probability of severing of highly curved microtubule regions and straight island-covered microtubule regions, within 150 s after the addition of katanin. The bars represent the probability averaged over n = 4 experiments (29 bends and 82 straight microtubules), error bars represent the S.D. Curved microtubule regions were always cut. **(E)** Fluorescence micrograph showing the tau-mEGFP signal on microtubules at 20 nM tau-mEGFP in solution. Tau islands have higher tau-mEGFP densities than the tau-mEGFP regions localizing to microtubule regions with high curvature. See quantification and number of experiments in (H). **(F)** Kymograph showing the uniform increase of tau-mEGFP density along the whole region of the microtubule curve upon the addition of tau-mEGFP in solution. This is in strong contrast to islands localized on straight microtubules, which grew at their boundaries. See quantification and number of experiments in (G). **(G)** Exemplary time-trace of tau density in the regions of high curvature after addition of 20 nM tau-mEGFP in solution (n = 5 microtubules, thick line and shaded area indicate the three quartiles). In contrast to the islands, in the high-curvature regions the tau density increases immediately after the addition of tau-mEGFP in solution (similar to the behavior in the regions surrounding the islands). We observed similar timescales in a total of n = 20 high-curvature regions in 5 experiments (6 ± 2 s for high-curvature regions, 8 ± 6 s for surroundings, weighted average ± S.D., each experiment has equal weight). **(H)** Densities of tau-mEGFP outside the islands, inside the islands and in the regions of high curvature at 20 nM tau-mEGFP in solution (n = 11 high-curvature regions in 5 experiments). Points are color-coded by experiments, horizontal lines indicate the three quartiles, weighted such that each experiment has equal weight. Scale bars, vertical 10 min, horizontal 2 µm.

Supplementary Tables | Supplementary Table 1: Experiment Statistics Source Data. Excel file containing all experiment statistics source data. For a detailed content description, please see Methods, section: Data Availability.

Supplementary Videos

Supplementary Video 1: Tau island formation. Formation of islands of high tau-mEGFP density on Atto647-labeled microtubule (not shown) after the addition of 20 nM tau-mEGFP. Experiment presented in Figure 1C.

Supplementary Video 2: Tau island disassembly. Disassembly of the tau-mEGFP islands upon removal of tau-mEGFP from solution. Experiment presented in Figure 1G (the frames before removing tau from solution are not shown in the kymograph).

Supplementary Video 3: Tau turnover inside and outside of islands. Tau turnover inside and outside the islands visualized after the exchange of 20 nM tau-mCherry (red) for 20 nM tau-mEGFP (green). Experiment presented in Figure 2A.

Supplementary Video 4: Tau islands shield microtubules from severing-enzymes. Katanin-GFP-mediated microtubule severing and subsequent microtubule disassembly occurred initially only outside the islands. On longer time scales, also the island-covered parts of the microtubules started disassembling from their boundaries. Experiment presented in Figure 4B.

Supplementary Video 5: Disassembly of islands by super-processive kinesins. Kip3-EGFP (green) moves, in the low tau-mEGFP density regions (dim red) and in the islands (bright red). Kip3-GFP that accumulated in front of a tau-mCherry island caused enhanced unbinding of tau-mCherry from the boundary of the island leading to complete disassembly of the island. Experiment presented in Figure 4C,D.

Supplementary Video 6: Tau cohesion within islands, not the mere density of tau, shields microtubules from being severed. Tau-mCherry at a concentration of 0.8 µM covers microtubules uniformly. Upon addition of Katanin-GFP, Katanin-GFP binds (and disassembles microtubules predominantly) in regions which are not shielded by tau islands (see also Supplementary Video 4). Experiment presented in Figure 5A.

Supplementary Video 7: Preferential binding of tau to curved microtubules is distinct from island formation. Katanin-GFP mediated severing of microtubules decorated with tau-mCherry islands (as in Supplementary Video 5). Please note that microtubule regions of high curvature are not protected from severing. Experiment presented in Supplementary Figure 5.